Synthesis and Characterization of a Cubic Iron Hydroxy Boracite

Stephanie C. Neumair[a], Johanna S. Knyrim[b], Oliver Oeckler[c], Reinhard Kaindl[d], and Hubert Huppertz[a]

[a] Institut für Allgemeine, Anorganische und Theoretische Chemie, Leopold-Franzens-Universität Innsbruck, Innrain 52a, 6020 Innsbruck, Austria
[b] Süd-Chemie AG, BU Performance Packaging, Ostenriederstraße 15, 85368 Moosburg, Germany
[c] Department Chemie, Ludwig-Maximilians-Universität München, Butenandtstraße 5 – 13, 81377 München, Germany
[d] Institut für Mineralogie und Petrographie, Leopold-Franzens-Universität Innsbruck, Innrain 52f, 6020 Innsbruck, Austria

Reprint requests to H. Huppertz. E-mail: Hubert.Huppertz@uibk.ac.at

Z. Naturforsch. **2011**, *66b,* 107 – 114; received November 16, 2010

The cubic iron hydroxy boracite $Fe_3B_7O_{13}OH \cdot 1.5\,H_2O$ was synthesized from Fe_2O_3 and B_2O_3 under high-pressure/high-temperature conditions of 3 GPa and 960 °C in a modified Walker-type multianvil apparatus. The crystal structure was determined at room temperature by X-ray diffraction on single crystals. It crystallizes in the cubic space group $F\bar{4}3c$ (Z = 8) with the parameters a = 1222.4(2) pm, V = 1.826(4) nm^3, R_1 = 0.0362, and wR_2 = 0.0726 (all data). The B-O network is similar to that of other cubic boracites.

Key words: Borate, Crystal Structure, Hydroxy Boracite, High Pressure

Introduction

Boracites have been extensively studied during the last two centuries [1]. The name boracite, which is actually used for more than 25 compounds, was attributed to the mineral $Mg_3B_7O_{13}Cl$ [2]. The general formula can be written as $M_3B_7O_{13}X$ with M = Mg, Cr, Fe, Co, Ni, Cu, Zn, Cd, or monovalent Li and X = Cl, Br, I [2], or occasionally OH, S, Se, Te, and F. As it is the rule, the specific boracites will be described here by their M and X ions, *e. g.* Mg-Cl stands for the boracite $Mg_3B_7O_{13}Cl$.

Besides varying chemical compositions, there are different structural modifications of boracite: the cubic high-temperature modification and several low-temperature modifications, which show either orthorhombic (low- or β-Mg-Cl, $Pca2_1$ [3]), trigonal (Fe-Cl, $R3c$ [3, 4]), tetragonal (Cr-Cl [5], $P\bar{4}2_1c$), or monoclinic symmetry (Fe-I below 30 K [6]). Due to their unique structure, some boracites have interesting physical properties like pyroelectricity (orthorhombic Mg-Cl [7,8]), piezoelectricity (cubic Mg-Cl [7,8]), ferroelectricity, ferroelasticity, and ferromagnetism (Fe-I below 30 K [6]). This led to several applications, *e. g.* as optic stopper [2, 9], ferroelectric non-volatile memory (ferroelectric random access memory or FRAM) [2, 10], and infrared (IR) detector [2, 11, 12].

Up to now, only a few hydroxy boracites are known, *e. g.* $Ni_3B_7O_{13}[I_{1-x}(OH)_x]$ [13], Mn-OH [14], Mg-OH [14], Fe-OH [13, 15], Cd-OH [16], and $CaMg[B_3O_4(OH)_3]_2 \cdot H_2O$ [17]. However, structural investigations were only carried out into the latter two, and the refinement of hydrogen atoms was successful only for $CaMg[B_3O_4(OH)_3]_2 \cdot H_2O$. Concerning Fe-OH, Kravchuk *et al.* [15] published X-ray powder data of crystals with colors from pale-grey to yellow, which do not correspond to our findings. Joubert *et al.* [13] only mentioned the successful synthesis of Fe-OH.

In the course of our research, we synthesized and examined a new blue Fe-OH boracite. In this paper, the synthesis, crystal structure, and properties of this compound are discussed and compared to those of other boracites.

Experimental Section

Synthesis

The iron borate Fe-OH was synthesized under high-pressure/high-temperature conditions of 3 GPa and 960 °C in a modified Walker-type multianvil apparatus. A mixture of Fe_2O_3 (Merck, Germany, 99 %) and partially hydrolyzed B_2O_3 (Strem Chemicals, Newburyport, USA, 99.9 %) in a molar ratio of 3 : 11 was ground together and filled into

0932–0776 / 11 / 0200–0107 $ 06.00 © 2011 Verlag der Zeitschrift für Naturforschung, Tübingen · http://znaturforsch.com

a boron nitride crucible (Henze BNP GmbH, HeBoSint® S100, Kempten, Germany). The crucible was positioned in the center of an 18/11-assembly and compressed by eight tungsten carbide cubes (TSM-10, Ceratizit, Reutte, Austria). The pressure was applied *via* a Walker-type multianvil device and a 1000 t press (both devices from the company Voggenreiter, Mainleus, Germany). A detailed description of the assembly and its preparation can be found in refs. [18–22]. To synthesize Fe-OH, the sample was compressed to 3 GPa within 65 min and kept at this pressure during the heating period. The temperature was increased in 5 min to 960 °C, kept there for 5 min, and lowered to 640 °C in 15 min. The sample was cooled to room temperature by switching off the heating, followed by a decompression period of 205 min. The recovered pressure medium was broken apart and the surrounding boron nitride crucible removed from the sample. The compound Fe-OH was obtained in the form of blue cubes, surrounded by amorphous B_2O_3. The excess of B_2O_3 served as a flux, leading to an increased crystal size of the Fe-OH boracite. To purify the air- and water-resistant Fe-OH, the sample was washed in hot water, which dissolved the boron oxide.

During the reaction of Fe_2O_3 and B_2O_3, the iron cations were reduced to the oxidation state 2+. A reduction of the metal ions to lower oxidation states or to the corresponding metal is often observed in the multianvil high-pressure assembly when hexagonal boron nitride and graphite are used as crucible and furnace materials, respectively [23], especially at elevated temperatures. A precise explanation of the redox mechanism with hexagonal boron nitride and graphite as reducing agents is still to be found.

The elemental analysis of Fe-OH through energy dispersive X-ray spectroscopy (Jeol JFM-6500F, Jeol. Ltd, Tokyo, Japan) led to values of 9.3 % Fe (12 %), 32 % B (28 %) and 58 % O (60 %) (theoretical values in parentheses).

Crystal structure analysis

For the single-crystal structure analysis, small irregularly shaped crystals of Fe-OH were isolated by mechanical fragmentation (unwashed). The measurements of the single-crystal intensity data were performed at r. t. on a Stoe IPDS-I diffractometer with graphite-monochromatized MoK_α (λ = 71.073 pm) radiation.

The determination of the metrics yielded a cubic F-centered unit cell. The Laue symmetry $m\bar{3}m$ and systematically absent reflections hhl with $h, l = 2n$ indicated the possible space groups $F\bar{4}3c$ and $Fm\bar{3}c$. As no solution could be obtained by Direct Methods, the structure was solved by trial and error. Taking into account the multiplicity of the Wyckoff positions in an F-centered unit cell with the Laue symmetry $m\bar{3}m$, it is clear that the maximum multiplicity of an iron site is limited to 24, because otherwise an unreasonably high density of > 4 g cm^{-3} would result. The refinement of an Fe position on the 24c site (0 1/4 1/4) in the space group $F\bar{4}3c$ yielded an R_1 value of ≈ 0.25. From this starting point, the light atoms could be located from subsequent Fourier and difference Fourier syntheses. However, the displacement parameter of Fe indicated a strong deviation from the 24c site. Assuming a half occupied split position 48g (x 1/4 1/4) with $x \approx 0.03$, the R values dropped significantly. No additional symmetry could be found, so the structure is non-centrosymmetric in accordance with all other cubic boracites; the Flack parameter converged to a value of $-0.02(7)$.

Table 1. Crystal data and numbers pertinent to data collection and structure refinement of $Fe_3B_7O_{13}OH \cdot 1.5\,H_2O$ (standard deviations in parentheses where applicable).

Empirical formula	$Fe_3B_7O_{13}OH \cdot 1.5\,H_2O$
Molar mass, g mol^{-1}	495.25
Crystal system	cubic
Space group	$F\bar{4}3c$
Crystal size, mm^3	$0.07 \times 0.10 \times 0.12$
Temperature, K	293(2)
Single crystal diffractometer	Stoe IPDS-I
Radiation	MoK_α (λ = 71.073 pm)
Single-crystal data	
a, pm	1222.4(2)
V, nm^3	1.8266(4)
Formula units per cell Z	8
Calculated density, g cm^{-3}	3.60
Absorption coefficient, mm^{-1}	4.8
F(000), e	1928
θ range, deg	3.3 – 30.2
Range in hkl	$-7 \le h \le 17$, $-17 \le k \le 10$, $-17 \le l \le 17$
Total no. of reflections	1930
Independent reflections / R_{int} / R_σ	238 / 0.0352 / 0.0195
Reflections with $I \ge 2\sigma(I)$	211
Data / ref. parameters	238 / 25
Absorption correction	numerical [24, 25]
Transm. ratio (min / max)	0.667 / 0.703
Goodness-of-fit on F^2	1.088
Final R_1 / wR_2 [$I \ge 2\sigma(I)$]	0.0312 / 0.0714
R_1 / wR_2 (all data)	0.0362 / 0.0726
Flack parameter x	$-0.02(7)$
Largest diff. peak / hole, e Å^{-3}	0.7 / -0.4

A numerical absorption correction was applied to the intensity data [24, 25]. The iron, boron, and oxygen atoms were refined with anisotropic displacement parameters [26]. Final difference Fourier syntheses did not reveal any significant peaks in the refinements. Details of the data collection and structure refinement are listed in Table 1. The positional parameters, anisotropic displacement parameters, interatomic distances, and interatomic angles are given in Tables 2 – 5.

Further details of the crystal structure investigation may be obtained from the Fachinformationszentrum Karlsruhe, 76344 Eggenstein-Leopoldshafen, Germany (fax: +49-7247-808-666; e-mail: crysdata@fiz-karlsruhe.de, http://

Atom	W. position	x	y	z	U_{eq}	*sof*
Fe	48*g*	0.03073(8)	1/4	1/4	0.0248(3)	0.5
B1	32*e*	0.0797(3)	x	x	0.025(2)	1
B2	24*d*	1/4	0	0	0.0105(7)	1
O1	96*h*	0.0231(2)	0.0965(2)	0.1821(2)	0.0145(4)	1
O2	8*a*	0	0	0	0.026(2)	1
O3	8*b*	1/4	1/4	1/4	0.054(4)	0.5
O4	32*e*	0.3103(7)	x	x	0.099(5)	0.5

Table 2. Atomic coordinates and equivalent isotropic displacement parameters U_{eq} (Å^2) of Fe-OH (space group: $F\bar{4}3c$) with standard deviations in parentheses. U_{eq} is defined as one third of the trace of the orthogonalized U_{ij} tensor.

Atom	U_{11}	U_{22}	U_{33}	U_{23}	U_{13}	U_{12}
Fe	0.0343(6)	0.0188(6)	0.0211(6)	−0.0034(6)	0	0
B1	0.025(2)	U_{11}	U_{11}	0.012(2)	U_{23}	U_{23}
B2	0.007(2)	0.012(2)	U_{22}	0	0	0
O1	0.0162(9)	0.0162(8)	0.0111(7)	0.0044(7)	0.0047(6)	0.0062(7)
O2	0.026(2)	U_{11}	U_{11}	0	0	0
O3	0.054(4)	U_{11}	U_{11}	0	0	0
O4	0.099(5)	U_{11}	U_{11}	−0.019(5)	U_{23}	U_{23}

Table 3. Anisotropic displacement parameters of Fe-OH (space group: $F\bar{4}3c$) with standard deviations in parentheses.

Table 4. Interatomic distances (pm) in Fe-OH (space group: $F\bar{4}3c$) calculated with the single-crystal lattice parameters (standard deviations in parentheses).

Fe–O1a	205.5(2)	2×	B1–O1	144.5(2)	3×
Fe–O1b	215.5(2)	2×	B1–O2	168.7(6)	1×
	+		av.	150.6	
Fe–O4	220.5(2)	2×	B2–O1	1.469(2)	4×
	or				
Fe–O3	268.0(2)	1×			

Table 5. Interatomic angles (deg) in Fe-OH (space group: $F\bar{4}3c$) calculated with the single-crystal lattice parameters (standard deviations in parentheses).

O1–B2–O1	108.6(1)	3×	O1–B1–O1	111.1(2)	3×
O1–B2–O1	111.2(2)	3×	O1–B1–O2	107.8(3)	3×
av.	109.9		av.	109.5	

www.fiz-informationsdienste.de/en/DB/icsd/depot_anforderung.html) on quoting the deposition number CSD-422340.

Vibrational spectra

The confocal Raman spectra of single crystals were obtained with a Horiba Jobin Yvon LabRam-HR 800 Raman micro-spectrometer. The samples were excited using the 488 nm emission line of a 14 mW Ar^+ laser and the 532 nm line of a 100 mW Nd-YAG laser. The size and power of the laser spot on the surface were approximately 1 μm and 2 – 5 mW, respectively. The spectral resolution, determined by measuring the Rayleigh line, was about 2 cm^{-1}. The dispersed light was collected by a 1024 × 256 open electrode CCD detector. The spectra were recorded unpolarized. Background and Raman bands were fitted by the built-in spectrometer software LabSpec to second order polynomial and convoluted Gaussian-Lorentzian functions, respectively. The accuracy of the Raman line shifts, calibrated by regularly measuring the Rayleigh line, was in the order of 0.5 cm^{-1}. Heating experiments were performed with a Linkam THMS 600 heating stage mounted to the Raman spectrometer. The crystals were placed in a quartz crucible and heated at a rate of 50 °C per minute up to 500 °C.

The FTIR-ATR (*A*ttenuated *T*otal *R*eflection) spectra of single crystals were recorded with a Bruker Vertex 70 FT-IR spectrometer (spectral resolution 4 cm^{-1}) attached to a Hyperion 3000 microscope in the spectral range 600 – 4000 cm^{-1}. A frustrum-shaped germanium ATR-crystal with a tip diameter of 100 μm was pressed on the surface of the borate crystal with a power of 5 N, which crushed it into pieces of μm-size. 64 scans of the sample and of the background were acquired. Beside the spectra correction for atmospheric influences, an enhanced ATR-correction [27], using the OPUS 6.5 software, was performed. A mean refraction index of the sample of 1.6 was assumed for the ATR-correction. Background correction and peak fitting were applied using polynomial and convoluted Gaussian-Lorentzian functions.

Results and Discussion

Crystal structure of $Fe_3B_7O_{13}OH \cdot 1.5\,H_2O$

The boracite structure of Fe-OH ($Fe_3B_7O_{13}OH \cdot 1.5\,H_2O$) is built up from star-like units of four distorted BO_4 tetrahedra sharing one common corner (oxygen). These star-shaped units are connected *via* additional, undistorted BO_4 tetrahedra to form a network structure. Fig. 1 shows the cubic unit cell of Fe-OH with the star-shaped unit (light polyhedra, yellow) and the connecting BO_4 tetrahedra (dark polyhedra, blue). The structure exhibits channels of *achter* rings (rings consisting of eight tetrahedral centers) [28], running along all three spatial directions, so that an open network is generated. Inside these channels, iron and oxygen ions are accomodated. Some of

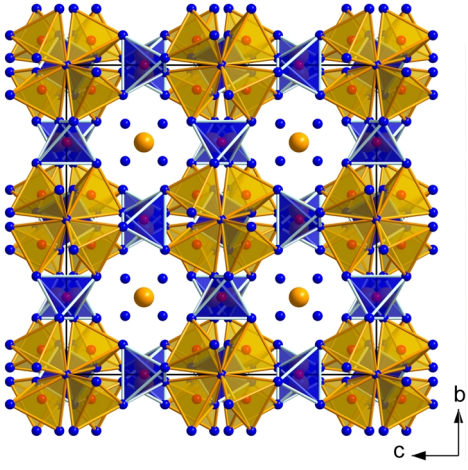

Fig. 1 (color online). Projection of the crystal structure of $Fe_3B_7O_{13}OH \cdot 1.5\,H_2O$. BO_4 tetrahedra: light (yellow) tetrahedra: star-like units; dark (blue) tetrahedra: connecting BO_4 tetrahedra; large (yellow) spheres: Fe^{2+}; corners of polyhedra and small dark spheres (blue spheres): O^{2-}; center of polyhedra (red spheres): B^{3+}.

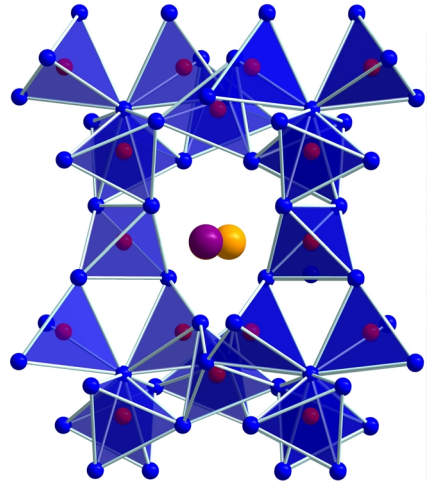

Fig. 2 (color online). Split position of Fe^{2+} in $Fe_3B_7O_{13}OH \cdot 1.5\,H_2O$; view along [110].

the positions inside the channels show a specific disorder, *e. g.* a displacement of the metal ions along the $\bar{4}$ axis of site 24*c* in Cd-S [29], or a four-fold disorder around the site 8*b* in Cd-S [29] and Li-Cl [30]. The same applies to our compound, where the iron and oxygen ions are disordered. For many cubic boracites it is argued that the disorder of the metal and halogen ions found in the structures is in doubt.

Nelmes and Hay [31] have shown that the metal cations in the cubic halogen boracites Cr-Cl [32], Ni-I [33], Cu-Cl, Co-I, and Cu-Br are not necessarily disordered. Several years later, R. O. Gould, R. J. Nelmes, and S. E. B. Gould [29] reported new results about the above mentioned cubic cadmium sulfur boracite Cd-S, where the Cd ions are clearly disordered over two sites more than 100 pm apart. The authors concluded that the occurrence of disorder in the cubic boracites seems to depend on the constituting elements and their interactions. So, obviously, the authors' most probable explanation seems to be the higher affinity of the Cd^{2+} ions for sulfur in contrast to the lower affinity of the above mentioned metal cations to the halide anions (Cr-Cl, Ni-I, Cu-Cl, Co-I, Cu-Br). A simple geometrical reason for the displacement to the off-center sites could not be given.

The iron boracite presented here exhibits a very pronounced disorder. Fig. 2 shows the two split positions of Fe^{2+} (view along [110]) shaded (colored) dark (violet) and light (orange). The oxygen anions inside the channels (O3) were positioned and refined on the site 8*b*. Further difference Fourier syntheses resulted in four peaks of electron density (site 32*e*) tetrahedrally arranged around the oxygen position O3. These peaks were already reported by Ito *et al.* for cubic Mg-Cl [8]. In order to explain these electron density peaks in Fe-OH, we assume a disorder of oxygen over the central site (O3, 8*b*) and the site 32*e* (O4). Fig. 3 shows the tetrahedral array of the partially occupied oxygen positions O3 and O4. The refinements with a variable occupation of the two different sites led to site occupation factors (*sof*) of 54 % for the "inner" position (O3, site 8*b*) and 44 % for the "outer" position (O4, 32*e*) (R_1 = 0.0356 and wR_2 = 0.0706 (all data)). Obviously, the distance between the two sites is too short (128(2) pm) for a simultaneous occupation with oxygen atoms, which corresponds to the refined *sof*. Thus, either site 8*b* or site 32*e* is occupied. Due to the fact that the *sof* were close to a 50 % occupation of the two sites, the occupancies were constrained to 50 % in the final refinements. This led to the formula $Fe_3B_7O_{15.5}$.

The IR and Raman spectra revealed intense O-H modes. As all known boracites show metal atoms in the oxidation state +2 and +1 (Li boracite), we also assume the oxidation state +2 for the iron boracite described here. Thus, for charge balance reasons, four H ions are required per formula unit. As O3 and O4 are not part of the B-O network, it is likely that these two oxygen ions bind to the hydrogen ions, forming

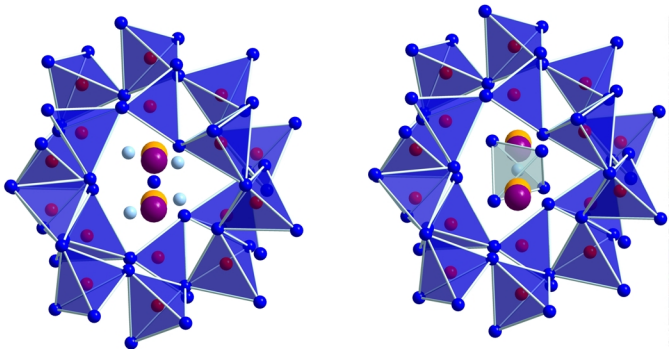

Fig. 3 (color online). Detail of the crystal structure of $Fe_3B_7O_{13}OH \cdot 1.5\,H_2O$: partial occupation of O3 and O4; left: the O3 site (small dark sphere, dark blue) is occupied, while the O4 site (small light spheres, light blue) remains unoccupied; right: the O3 site (small light sphere, light blue) is unoccupied, while all O4 sites (small dark spheres, dark blue) are occupied.

OH^- or water molecules. In cubic boracites, site 8*b* (O3) typically represents the anion site (position of Cl in Mg-Cl). Thus, hydroxyl groups seem plausible at this site. A possible structural model would suggest an equilibrium of the negative charges on the two sites (O3, 8*b*; O4, 32*e*). Therefore, we propose a model in which the oxygen atoms O3 (site 8*b*) bind to hydrogen atoms, forming hydroxyl groups. Concerning the 32*e* site (O4), one negative charge has to be shared by four occupied oxygen positions, which can be achieved by a model of one OH^- group and three H_2O molecules for the site 32*e* (O4). Due to the half occupied sites 8*b* ($0.5\,OH^-$) and 32*e* ($0.5\,OH^- + 1.5\,H_2O$), this sums up to the formula "$Fe_3B_7O_{13}OH \cdot 1.5\,H_2O$". As it was not possible to locate the position of the hydrogen atoms by X-ray crystal structure analysis, this model relies on vibrational spectroscopic measurements and the above reasoning. The shortest O4···O1 distances have values of 281.14(2) (3×) and 284.02(3) pm (3×), which is in good agreement with the O···O distances in solid water (275 pm [34]). Thus, hydrogen ions can be expected to lie between O4 and O1, forming hydrogen bridges. The interatomic distance between the O4 sites is 208.65(2) pm, which is rather short for HO-H···OH^- distances (229 pm [34]). As stated above, crystals of Fe-OH had to be washed in water to gain larger quantities of the pure phase. The open network structure possibly has a variable content of water, influenced by the washing with water. Thus, measurements of the H_2O content in Fe-OH by means of DTA would not be informative.

As pointed out above, Fe-OH exhibits a pronounced split position of the Fe^{2+} ions. Fig. 4 depicts the coordination sphere of the iron ions in Fe-OH; Table 4 lists the Fe-O distances. Due to the displacement to the off-centered sites, the iron ions show a distorted sixfold coordination or a distorted 4+1 coordination determined

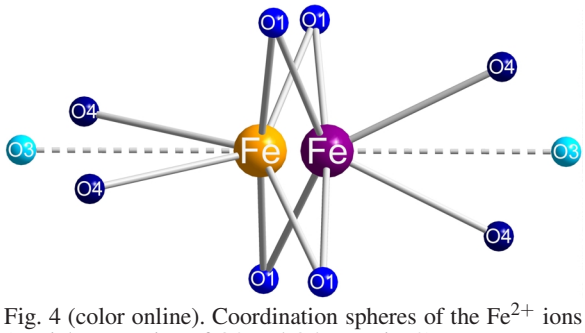

Fig. 4 (color online). Coordination spheres of the Fe^{2+} ions (partial occupation of O3 and O4; see Fig. 3).

by the occupation of the sites O4 (32*e*) or O3 (8*b*), respectively. The enlarged coordination sphere as compared to the usually fourfold coordinated metal sites in cubic boracites (C.N. = 4, distorted tetrahedron), appears to be favored under high-pressure conditions, which thus may also be a reason for the splitting. As stated in ref. [31] for Cd-S, the most probable explanation for the pronounced positional spliting is the higher affinity of Fe^{2+} to oxygen in contrast to the lower affinity of other metal cations to the corresponding halide anions.

The blue color of the Fe-OH crystals implies that there is a certain amount of Fe^{3+} ions incorporated in the structure. The mineral vivianite ($Fe^{2+}{}_3(PO_4)_2 \cdot 8\,H_2O$) has an indigo-blue color, which results from an $Fe^{2+} \rightarrow Fe^{3+}$ intervalence charge transfer (IVCT). The chemical formula of this compound does not indicate a mixed-valence, but freshly prepared pale-green crystals of vivianite rapidly turn blue, when exposed to air, which is due to the partial oxidation of Fe^{2+} [35]. As there was no color change when Fe-OH was exposed to air, the small amount of Fe^{3+} ions might come from the starting material. It is reasonable to suppose that charge imbalances caused by Fe^{3+} can be compensated by the

generation of OH^- from water molecules in the crystal structure.

In 1981, Gould *et al.* [29] published a cubic cadmium sulfur boracite with similar features. The Cd ions are disordered over two sites. The site 8*b*, where the S ions are situated, is tetrahedrally surrounded by four peaks of electron density. In this case, the electron density distribution was interpreted as a disordered "S_2^{2-}" ion with one S at the central site 8*b* and the other one distributed uniformly over the four surrounding sites (32*e*). In order to compare the model of Gould *et al.* with our data set, we refined our single crystal data by constraining the *sof* to the values found for Cd-S (O3: 100 %, O4: 25 %). This resulted in increased residual factors (R_1 = 0.045 and wR_2 = 0.1066 (all data)) compared to our model (R_1 = 0.0362 and wR_2 = 0.0726 (all data)). Thus, the model of Gould *et al.* does not fit to our data for Fe-OH. In this context, it is noteworthy that in the cubic Li-*X* boracites [30], the *X* site is also surrounded by four peaks of electron density. These peaks are occupied with the additional lithium ion, disordered over the four positions, which is needed for charge balance.

Since cubic boracites are usually synthesized in closed silica glass ampoules at elevated temperatures [4,36], the assumption stands to reason, if Fe-OH is a normal-pressure phase or a metastable high-pressure phase.

Vibrational spectroscopy

The IR-absorbance and Raman spectra of single crystals of Fe-OH are displayed in Figs. 5 and 6, respectively. The assignment of the vibrational modes is based on the comparison with the experimental data of borate crystals and glasses containing BO_3 and BO_4 units [37–42]. According to Moopenn and Coleman [43], internal vibrational modes of the borate framework occur at wavenumbers above 200 cm^{-1}. Bands up to 800 cm^{-1} can be assigned to bending and stretching vibrations of various borate arrangements, while bands in the region 800 – 1600 cm^{-1} are typical for stretching vibrations of B-O units. Absorptions of BO_4 tetrahedra are expected at wavenumbers of 800 – 1100 cm^{-1} [44–46], whereas those of BO_3 groups dominate at 1200 – 1450 cm^{-1} [47–50]. However, due to the different structure and the interconnecting metal cations, assignments remain tentative to a certain degree [51].

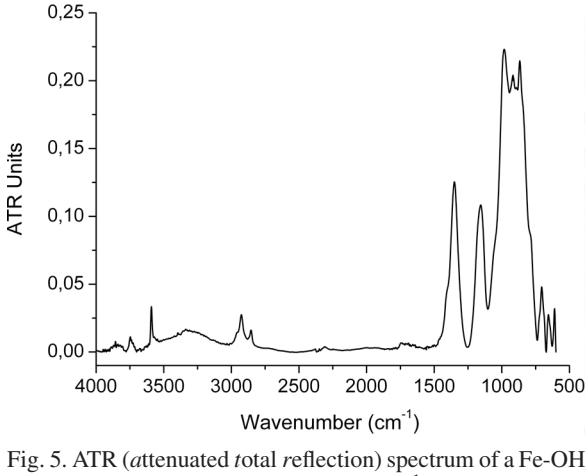

Fig. 5. ATR (*a*ttenuated *t*otal *r*eflection) spectrum of a Fe-OH single crystal in the range 4000 – 500 cm^{-1}.

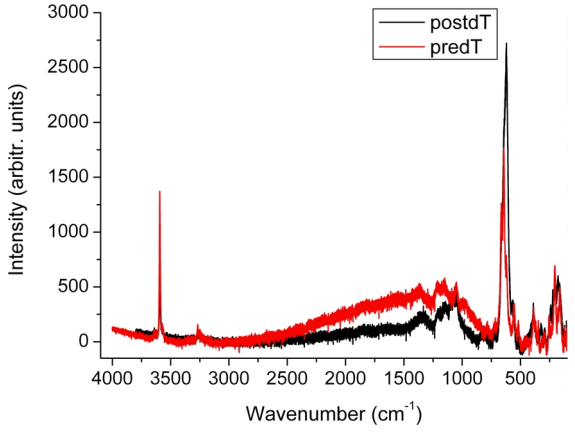

Fig. 6 (color online). Confocal Raman spectra of a Fe-OH single crystal in the range 4000 – 100 cm^{-1} before (grey / red) and after heating to 500 °C (black).

Several cubic boracites and their phase transitions were investigated by vibrational spectroscopy in the last thirty years [52–54]. Interestingly, cubic boracites show absorption bands in a frequency range of 1200 – 1400 cm^{-1}, where usually those of BO_3 triangles occur. As cubic boracites exhibit only BO_4 groups, the authors in ref. [52] discussed, whether BO_3 triangles do persist in the cubic high-temperature form after the phase transition. For a better understanding of the phonon band structure in cubic boracites, Iliev *et al.* [54] performed DFT (density functional theory) calculations for Raman modes and showed that for cubic Co-Cl vibrational bands of distorted OBO_3 tetrahedra can be expected in the range of 1150 – 1300 cm^{-1}.

Fig. 5 depicts the IR-ATR-spectrum of Fe-OH, which shows strong absorbance at 800 – 1000, 1200,

and 1350 cm^{-1}. As stated above, the strong modes can be assigned to vibrations of the B-O network. The band at 1350 cm^{-1} is associated with the antisymmetric stretching mode of the distorted BO_4 tetrahedra. Above 1500 cm^{-1}, several groups of weaker bands are detected, which confirm the presence of crystal water in the structure. In the region of 1600 – 1750 cm^{-1}, H-O-H bending of the crystal water occurs [40]. Modes at 2300 – 2350 and 3600 – 3800 cm^{-1} can be assigned to O-H stretching, and bands at 2800 – 3000 cm^{-1} belong to CH vibrations due to contaminations with silicone oil.

The Raman spectra of Fe-OH (Fig. 6) are characterized by the most intense lines at 700 and 3600 cm^{-1}. Additionally, several groups of lines are detected below 500, around 800, and in the range 1100 – 1400 cm^{-1}. As this cubic boracite exhibits only regular BO_4 and distorted OBO_3 tetrahedra, the lines at 800 cm^{-1} have to be assigned to the stretching modes of the BO_4 tetrahedra, while the stretching modes of distorted OBO_3 tetrahedra absorb in the region of 1100 – 1400 cm^{-1}. The strong line at 3600 cm^{-1} is typical for the OH mode of water-containing borates, thus confirming the presence of crystal water in the structure [55]. The weaker lines around 3250 cm^{-1} are probably related to CH vibrations of impurities [56] and disappear almost completely after heating (see below). Fig. 6 shows two Raman spectra: before (grey / red) and after (black) heating to 500 °C. Apparently, the crystal water could be partly expelled without any obvious structural changes.

Conclusions

The cubic compound Fe-OH exhibits a B-O network comparable to that of other cubic boracites, with the iron atoms disordered over two sites, and the OH position – at the halide position in metal-halogen boracites – tetrahedrally surrounded by partially occupied oxygen atom positions. The model presented here leads to the formula of $Fe_3B_7O_{13}OH \cdot 1.5\,H_2O$. IR and Raman measurements have shown intense O-H modes that confirm the water content.

Acknowledgements

We gratefully acknowledge the continuous support of this work by Prof. Dr. W. Schnick, Department Chemie of the University of Munich (LMU). Special thanks go to Dr. P. Mayer for collecting the single-crystal data. This work was financially supported by the Deutsche Forschungsgemeinschaft (HU 966/2-3) and the Fonds der Chemischen Industrie.

[1] A. G. Werner, *Bergmännisches Journal* **1789**, 393.
[2] J. Campa-Molina, S. Ulloa-Godinez, A. Barrera, L. Bucio, J. Mata, *J. Phys.: Condens. Matter* **2006**, *18*, 4827.
[3] E. Dowty, J. R. Clark, *Solid State Commun.* **1972**, *10*, 543.
[4] M.-E. Mendoza-Alvarez, K. Yvon, W. Depmeier, H. Schmid, *Acta Crystallogr.* **1985**, *C41*, 1551.
[5] H. K. Mao, F. Kubel, H. Schmid, K. Yvon, *Acta Crystallogr.* **1991**, *B47*, 692.
[6] F. Kubel, *Ferroelectrics* **1994**, *160*, 61.
[7] H. Schmid, *J. Phys. Chem. Solids* **1965**, *26*, 973.
[8] T. Ito, N. Morimoto, R. Sadanaga, *Acta Crystallogr.* **1951**, *4*, 310.
[9] L. Smart, E. Moore, *Solid State Chemistry, An Introduction*, Chapman and Hall, London, **1992**.
[10] S. Matthews, R. Ramesh, T. Venkatesan, J. Benedetto, *Science* **1997**, *276*, 238.
[11] J. Campa-Molina, A. G. Castellanos-Guzman, M. Barcena-Soto, J. Reyes-Gomez, *Solid State Commun.* **1994**, 89, 963.
[12] J. Campa-Molina, O. Blanco, A. Correa-Gomez, M. Czank, A. G. Castellanos-Guzman, *J. Microsc.* **2002**, *208*, 201.
[13] J. C. Joubert, J. Muller, C. Fouassier, A. Levasseur, *Kristall und Technik* **1971**, *6*, 65.
[14] J. C. Joubert, J. Muller, M. Pernet, B. Ferrand, *Bull. Soc. Fr. Minéral. Cristallogr.* **1972**, *95*, 68.
[15] T. A. Kravchuk, Yu. D. Lazebnik, *Russ. J. Inorg. Chem.* **1967**, *12*, 21.
[16] U. Werthmann, H. Gies, J. Glinnemann, Th. Hahn, *Z. Kristallogr.* **2000**, *215*, 393.
[17] C. Sabelli, A. Stoppioni, *Can. Mineral.* **1978**, *16*, 75.
[18] N. Kawai, S. Endo, *Rev. Sci. Instrum.* **1970**, *8*, 1178.
[19] D. Walker, M. A. Carpenter, C. M. Hitch, *Am. Mineral.* **1990**, *75*, 1020.
[20] D. Walker, *Am. Mineral.* **1991**, *76*, 1092.
[21] D. C. Rubie, *Phase Transitions* **1999**, *68*, 431.
[22] H. Huppertz, *Z. Kristallogr.* **2004**, *219*, 330.
[23] J. S. Knyrim, J. Friedrichs, S. Neumair, F. Roeßner, Y. Floredo, S. Jakob, D. Johrendt, R. Glaum, H. Huppertz, *Solid State Sci.* **2008**, *10*, 168.
[24] X-SHAPE (version 1.05), Crystal Optimisation for Nu-

merical Absorption Correction, Stoe & Cie GmbH, Darmstadt (Germany) **1999**.
[25] W. Herrendorf, H. Bärnighausen, HABITUS, Program for Numerical Absorption Correction, Universities of Karlsruhe and Giessen, Karlsruhe, Giessen (Germany) **1993/1997**.
[26] G. M. Sheldrick, *Acta Crystallogr.* **2008**, *A64*, 112.
[27] F. M. Mirabella, Jr. in *Internal Reflection Spectroscopy, Theory and Applications* (Ed.: F. M. Mirabella, Jr.), Marcel Dekker, New York, **1993**, p. 17.
[28] F. Liebau, *Structural Chemistry of Silicates*, Springer-Verlag, Berlin, **1985**.
[29] R. O. Gould, R. J. Nelmes, S. E. B. Gould, *J. Phys. C: Solid State Phys.* **1981**, *14*, 5259.
[30] W. Jeitschko, T. A. Bither, P. E. Bierstedt, *Acta Crystallogr.* **1977**, *B33*, 2767.
[31] R. J. Nelmes, W. J. Hay, *J. Phys. C: Solid State Phys.* **1981**, *14*, 5247.
[32] R. J. Nelmes, F. R. Thornley *J. Phys. C: Solid State Phys.* **1974**, *7*, 3855.
[33] F. R. Thornley, N. S. J. Kennedy, R. J. Nelmes, *J. Phys. C: Solid State Phys.* **1976**, *9*, 681.
[34] A. F. Holleman, E. Wiberg, N. Wiberg, *Lehrbuch der Anorganischen Chemie*, Walter de Gruyter, Berlin, New York, **2007**.
[35] R. G. Burns, *Mineralogical Applications of Crystal Field Theory*, 2nd ed., Cambridge University Press, Cambridge, **1993**.
[36] H. Schmid, *J. Phys. Chem. Solids* **1965**, *26*, 973.
[37] F. C. Hawthorne, P. C. Burns, J. D. Grice in *Boron: Mineralogy, Petrology and Geochemistry*, Vol. 33, 2nd ed. (Eds.: E. S. Grew, L. M. Anovitz), Mineralogical Society of America, Washington, **1996**, p. 41.
[38] H. Huppertz, *J. Solid State Chem.* **2004**, *177*, 3700.
[39] G. Chadeyron, M. El-Ghozzi, R. Mahiou, A. Arbus, J. C. Cousseins, *J. Solid State Chem.* **1997**, *128*, 261.
[40] L. Jun, X. Shuping, G. Shiyang, *Spectrochim. Acta A* **1995**, *51*, 519.
[41] G. Padmaja, P. Kistaiah, *J. Phys. Chem. A* **2009**, *113*, 2397.
[42] J. C. Zhang, Y. H. Wang, X. Guo, *J. Lumin.* **2007**, *122 – 123*, 980.
[43] A. Moopenn, L. B. Coleman, *J. Phys. Chem. Solids* **1990**, *51*, 1099.
[44] M. Ren, J. H. Lin, Y. Dong, L. Q. Yang, M. Z. Su, L. P. You, *Chem. Mater.* **1999**, *11*, 1576.
[45] J. P. Laperches, P. Tarte, *Spectrochim. Acta* **1966**, *22*, 1201.
[46] G. Blasse, G. P. M. van den Heuvel, *Phys. Stat. Sol.* **1973**, *19*, 111.
[47] S. D. Ross, *Spectrochim. Acta A* **1972**, *28*, 1555.
[48] W. C. Steele, J. C. Decius, *J. Chem. Phys.* **1956**, *25*, 1184.
[49] R. Böhlhoff, H. U. Bambauer, W. Hoffmann, *Z. Kristallogr.* **1971**, *133*, 386.
[50] K. Machida, H. Hata, K. Okuno, G. Adachi, J. Shiokawa, *J. Inorg. Nucl. Chem.* **1979**, *41*, 1425.
[51] L. Nasdala, D. Smith, R. Kaindl, M. Ziemann in *Spectroscopic Methods in Mineralogy*. Eötvös University Press, Budapest, **2004**, pp. 281 – 343.
[52] P. C. Burns, M. A. Carpenter, *Can. Mineral.* **1997**, *35*, 189.
[53] A. F. Murray, D. J. Lockwood, *J. Phys. C: Solid State Phys.* **1978**, *11*, 2349.
[54] M. N. Iliev, V. G. Hadjiev, J. Íñiguez, J. Pascual, *Acta Phys. Pol.* **2009**, *116*, 19.
[55] H.-Y. Sun, W. Sun, Y.-X. Huang, J.-X. Mi, *Z. Anorg. Allg. Chem.* **2010**, *636*, 977.
[56] B. Schrader, *Raman/Infrared Atlas of Organic Compounds*, 2nd ed. Wiley-VCH, Weinheim, **1989**.